Environmental Modelling and Software 155 (2022) 105450

Contents lists available at ScienceDirect

Environmental Modelling and Software

journal homepage: www.elsevier.com/locate/envsoft

Can re-infiltration process be ignored for flood inundation mapping and prediction during extreme storms? A case study in Texas Gulf Coast region

Zhi Li [a], Mengye Chen [a,*], Shang Gao [a], Yixin Wen [c,d], Jonathan J. Gourley [b], Tiantian Yang [a], Randall Kolar [a], Yang Hong [a,**]

[a] School of Civil Engineering and Environmental Science, The University of Oklahoma, Norman, OK, 73072, USA
[b] NOAA National Severe Storms Laboratory, Norman, OK, 73072, USA
[c] Cooperative Institute for Mesoscale Meteorological Studies, Norman, OK, 73072, USA
[d] Department of Geography, The University of Florida, Gainesville, FL, 21611, USA

ARTICLE INFO

Keywords:
Flood inundation modeling
Run-on infiltration
Re-infiltration
Soil moisture
Hydrologic-hydraulic modeling
Extreme flood events
Hurricane harvey
Bayou river basin

ABSTRACT

Coupled Hydrologic & Hydraulic (H&H) models have been widely applied for flood simulations, yet the modern H&H models suffer from one-way and weak coupling and particularly disregarded run-on infiltration, which could compromise the model accuracy. In this study, we assess the H&H model performance with and without re-infiltration process in extreme flooding events. Results highlight that the re-infiltration process should not be disregarded even in extreme flood simulations. Saturated hydraulic conductivity and antecedent soil moisture are found to be the prime contributors to such differences. For the Hurricane Harvey event, the model performance is verified against stream gauges and high water marks, from which the re-infiltration scheme increases the Nash Sutcliffe Efficiency score by 140% on average and reduces maximum depth differences by 17%. Meanwhile, the recent update of the CREST-iMAP model Version 1.1, which incorporates two-way coupling and re-infiltration scheme, is released for public access.

1. Introduction

Flooding, as a costly natural hazard, has been increasingly threatening human lives and economies (Gourley et al., 2017; Hirabayashi et al., 2013; Li et al., 2021a). In the United States, most billion-dollar natural hazards are tied to either local or regional flooding, making it the major cost to human society. Unfortunately, under a warmer climate with anthropogenic pressure, flood crises are likely to continue expanding, as the flood frequency accelerates and flood magnitude rises (Bates et al., 2021; Hirabayashi et al., 2013; Li et al., 2022a; Tabari, 2020; Triet et al., 2020; Swain et al., 2020; Viero et al., 2019). To combat flood risks, researchers have been developing hydrologic/hydraulic models to deliver accurate and timely flood information for local communities and decision-makers (Gourley et al., 2017). In the United States, two pronounced flood forecasting systems – the NWM (National Water Model) (Cohen et al., 2018; Viterbo et al., 2020) and FLASH (Flooded Locations And Simulated Hydrographs Project) (Gourley et al., 2017; Yussouf et al., 2020) – are capable of both simulating real-time floods and forecasting floods in a short range.

These large-scale flood monitoring systems, although claimed to offer inundation maps and predictions, weaken their hydrodynamic simulation due to computational constraints. For instance, the NWM adopts the Height Above Nearest Drainage (HAND) method to produce flood inundation maps along the river channels by mapping discharge to stage via rating curves (Johnson et al., 2019). This conceptual method, however, overlooks the physics of floodwater propagation because of no flow dynamics being represented (Wing et al., 2017). Moreover, it cannot simulate the pluvial flood, which is a local effect caused by intense rainfall rates and does not normally occur along river channels (Bates et al., 2021). More recently, some emerging hydrodynamic models have been successfully deployed and evaluated at continental or global scales (Bates et al., 2021; Grimaldi et al., 2019; Sampson et al., 2015; Wing et al., 2017; Yamazaki et al., 2011). These models simplify the full Shallow Water Equation (SWE) to speed up the flood simulation. Nevertheless, they normally do not represent the hydrologic process well, especially for the infiltration process, which is proven to be critical

* Corresponding author.
** Corresponding author.
E-mail addresses: mchen15@ou.edu (M. Chen), yanghong@ou.edu (Y. Hong).

https://doi.org/10.1016/j.envsoft.2022.105450
Received 19 October 2021; Received in revised form 21 April 2022; Accepted 15 June 2022
Available online 19 June 2022

in flood simulations (Li et al., 2021b; Ni et al., 2020). As such, a coupled physically-based hydrologic & hydraulic (H&H) model appears to be a better choice, which takes the complementary advantages for accurate flood modeling (Dullo et al., 2021; Felder et al., 2017; Kim et al., 2012; Nguyen et al., 2016; Pontes et al., 2017; Sebastian et al., 2021). Readers are referred to Teng et al. (2017) and Grimaldi et al. (2019) for a detailed review of coupled models. Most of such models, however, adopt one-way and weak coupling, meaning that there is no interplay between the hydrologic component and hydraulic component (Bravo et al., 2012). They normally produce surface runoff outputs first to drive the hydraulic model. The recent development of the Coupled Routing and Excess STorage inundation MApping and Prediction (CREST-iMAP) version 1.0 also uses this one-way coupling strategy (Chen et al., 2021; Li et al., 2021b).

Two-way coupling for the H&H models has not hitherto been well-recognized. The accumulated surface water (hydraulic feature), along with excess surface runoff during a flood event in principle would alter infiltration rates, whereby both the flood magnitudes and timings could differ. Therefore, we activate the surface water infiltration along its way to downslope, which is called run-on infiltration or re-infiltration in short (Smith and Hebbert, 1979; Nahar et al., 2004; Zhang et al., 2020). Nahar et al. (2004) defined this re-infiltration as the infiltration of surface water that, as it moves downslope, encounters areas where moisture deficit has not yet been satisfied. It is often ignored in rainfall-runoff studies, while it can be significant when the random nature of infiltration properties is taken into account (Corradini et al., 1998; Nahar et al., 2004). Smith and Hebbert (1979) simulated the run-on process with varying saturated hydraulic conductivity and rainfall rates, and they reported that the effect of the run-on process is to decrease the ponding time dramatically. Corradini et al. (2002) compared models with and without re-infiltration, and they suggested that re-infiltration greatly reduces surface flow and alters both rising and recession limbs of the hydrograph. Nahar et al. (2004) emphasized the influence of re-infiltration in hillslope hydrograph using the Green-Ampt model with a 1D kinematic wave surface routing. A recent study by Zhang et al. (2020) takes it one step further, in which they applied the community model WRF-Hydro (Weather Research Forecasting model-Hydrological modeling system) to explore the influence of rainfall rates, topography, soil types on the re-infiltration process. However, none of these studies have considered the implication of re-infiltration to hydrodynamic studies, where the overland flow is driven by the 2D Shallow Water Equation (SWE) instead of 1D routing. To do so, we can obtain a more realistic view of how re-infiltration plays a role in flood simulations.

During extreme flood events, the infiltration process is often disregarded because the infiltration rates are relatively low compared to excess rainfall rates. Yet, some studies claim that the infiltration process is critical to determine flood wave propagation, such as arrival and dissipation, especially in flat plain or regions with highly permeable soil media (Corradini et al., 2002; Mahapatra et al., 2020; Nahar et al., 2004; Li et al., 2021b; Woolhiser et al., 1996). A hydrodynamic model without infiltration is likely to overestimate flood depth (Kim et al., 2012; Li et al., 2021b; Ni et al., 2020). Nevertheless, it still remains unclear, or at least not as clear as infiltration, whether re-infiltration is essential for H&H models in extreme flood events. In other words, whether it is worth encapsulating such a scheme in modern flood simulation frameworks. To our knowledge, few studies have attempted to answer this question under the context of extreme flood events. Moreover, further questions can arise as to what the determining factors are during such a process and how it interacts with both flood magnitude and dynamics. **In light of these questions, the objectives of this study are to explore 1) the effectiveness and importance of the re-infiltration scheme to an H&H model, 2) the contributing factors to the differences between with and without re-infiltration, and 3) whether and to what extent the re-infiltration process can help improve flood inundation mapping and prediction of extreme events.** We first test its effectiveness and importance on a 100-year design extreme rainfall event during a sensitivity test and then apply it to a real case study – Hurricane Harvey – to validate the efficacy. It is anticipated to provide insightful information for model developers and researchers to understand the importance of the re-infiltration process to flood modeling. In this study, we also release our latest development of CREST-iMAP V1.1, which features a two-way coupling and re-infiltration scheme on top of the previous version (Chen et al., 2021; Li et al., 2021b).

The rest of this paper is structured as follows. Section 2 introduces the study area and necessary datasets for the model setup, followed by experimental designs. Section 3 presents the results from the sensitivity test and the Hurricane Harvey event. Section 4 discusses limitations of this study as well as recommendations for input data and future model development. At last, Section 4 concludes the main findings of this study.

2. Methods

2.1. Forcing data

Precipitation is the major driver of local or regional flooding, and it is thus central to acquire an accurate and high-resolution dataset. In the U. S., the Multi-Radar Multi-Sensor (MRMS) precipitation product, developed at the National Severe Storms Laboratory (NSSL), provides 2-min and 1-km rainfall field, making it suitable for flash flood forecasting (Yussouf et al., 2016). It integrates ~180 WSR-88D operational radars, creating a seamless radar mosaic across the CONUS and southern Canada. Recent studies (e.g., Chen et al., 2020; Li et al., 2020) verified the efficacy of MRMS data when compared to gauge-based and satellite-based products during the Hurricane Harvey event. The advantage of using radar rainfall is obvious for flood inundation modeling, as conventional rain gauges cannot readily represent the spatially variable rainfall fields. The MRMS data was downloaded at https://mtarchive.geol.iastate.edu/.

Besides precipitation data, potential evapotranspiration (PET) is a common input into a hydrologic system when the surface radiation is not resolved in the modeling process. In this real-case study, we obtain the PET data from the USGS FEWS data port (https://earlywarning.usgs.gov/fews) at daily temporal and 1° spatial resolution (Allen et al., 1998).

2.2. Environmental data

The modeling system requires inputs from the terrain, Land Use Land Cover (LULC), and soil type and depth. Among these variables, terrain data arguably plays the utmost important role in hydraulic simulation (Dullo et al., 2021; Schumann and Bates, 2018). There has been a thorough investigation of terrain data affecting flood inundation modeling since the early development of hydrologic/hydraulic models (Kenward et al., 2000; Sanders, 2007). Lately, with the increasing interest in deploying macro-scale flood inundation simulations, global terrain data assessment has been again brought up (Mohanty et al., 2020; Sampson et al., 2015). Generally, three types of data are favored and available in the U.S.: 1) airborne light ranging and detection (LiDAR) that resolves terrain with a high degree of vertical accuracy (0.05–0.2 m) and comes with a high spatial resolution but limited areal coverage, 2) spaceborne radar interferometry (IfSAR, e.g., Shuttle Radar Terrain Mission) that provides global coverage but poor vertical accuracy (~10 m) and spatial resolution (~90 m), and 3) a mixed product such as the National Elevation Dataset (NED) from the USGS that merges LiDAR surveys and the USGS quadrangle maps, whose accuracy (~5–7 m) and resolution (~5/10/30 m) sit in between the former two products. A general consensus from these studies is that LiDAR data is the most favorable DEM owing to improved vertical accuracy in flood modeling (Mohanty et al., 2020; Sanders, 2007; Schumann and Bates, 2018) but they have to be accompanied by surveyed channel profile since channel depth is not reflected. IfSAR, however, degrades its quality

because of poor vegetation penetration and speckle noise while the NED smooths some artifacts. The NED 10 m data accurately represents the river channel morphology than high-resolution LiDAR data that cannot penetrate water surface. Therefore, in this study, we select the 10 m DEM data from the NED dataset in the study area. To confirm the river channel bathymetry, 13 surveyed river geometries from the Harris Country Flood Control are curated and compared to NED 10 m, shown in Table 1. The average difference is found to be small (~0.55 m).

The LULC and impervious area data are acquired from the National Land Cover Database (NLCD) at 30 m resolution to derive a-priori parameter sets. The soil type dataset is retrieved from the United States Department of Agriculture.

2.3. Study area

Greens Bayou Basin, located in the north of the Houston metropolitan region, is one of the areas that are susceptible to regional flooding because, firstly, landfalling tropical cyclones and hurricanes bring torrential rainfall within a short period; secondly, the urban development in the recent years have altered the local ecosystem (e.g., replacement of soil with built-up structures). The basin is relatively flat (~1.5%), with an average elevation of around 23.65 m, and the total drainage area is 457.9 km^2. Three main streams flow across this region. Reinhardt Bayou (drainage area: 86.3 km^2) flows from north to south, met with Greens Bayou to form the longest river in this area. Halls Bayou (drainage area: 225.1 km^2), the second-longest river, meets Greens Bayou at the basin outlet (Fig. 1a). The five USGS stream gauges, situated at each mainstream, monitor instantaneous streamflow at a 15-min time interval. Nearly 90% of the area is well-developed, especially in the western portion; forests and wetlands are present downstream, close to the basin outlet (Fig. 1b). The soil types are dominated by a mixture of sand, clay, and loam (Fig. 1c). The typical runoff generation mechanism in this region is infiltration excess runoff when extreme rain rates surpass soil infiltration capacity, indicated by relatively low hydraulic conductivity values (Buchanan et al., 2018). Meanwhile, the correlation between rainfall and streamflow is above 0.6, pointing to a flashy hydrograph (Berghuijs et al., 2016).

During the 500-year Hurricane Harvey event, this region is largely inundated due to record-breaking 1600 mm rainfall over a one-week storm lifespan (Chen et al., 2020; Li et al., 2020). According to the Harris Country flood report, both Greens Bayou and Halls Bayou experienced a 500-year water level downstream and 50-year to 100-year in between upstream. Greens Bayou broke previous water level records in 2002 and observed flooding occurred along the entire channel.

2.4. CREST-iMAP model

Hydrologic modeling is thus far a common approach to deliver timely flood information for the sake of scalability and efficiency (Gourley et al., 2017). Yet, conventional hydrologic models bear large uncertainties in such developed regions, which is mainly due to 1) simplified representation of terrain (Dullo et al., 2021) and 2) one-dimensional routing that raises issues in flat regions (Flamig et al., 2020; Getirana and Paiva, 2013; Li et al., 2021b). On the other hand, hydraulic models do not excel in representing hydrologic processes. In light of these issues, the newly developed Coupled Routing and Excess STorage inundation MApping and Prediction (CREST-iMAP) model is used to investigate the importance of the re-infiltration scheme in flood inundation models. The CREST-iMAP integrates CREST V2.1 for the hydrologic part that simulates vertical water distribution by land surface and ANUGA V2.1 for the hydraulic routing that distributes spatial water over terrain by solving 2D shallow water equation. Its performance has been evaluated in this region against the non-coupled hydrologic models and other popular coupled models – WRF-Hydro + HAND and LISFLOOD FP (Chen et al., 2021; Li et al., 2021b). CREST-iMAP achieves similar performance with LISFLOOD-FP, if not better, and generally outperform WRF-Hydro + HAND. However, the previous version of CREST-iMAP V1.0 does not include the re-infiltration scheme, meaning that surface running water is not allowed to re-enter the soil. Here, we release the CREST-iMAP V1.1, an upgrade version, which considers two-way coupling via exchanging surface water between the hydraulic and hydrologic module and re-infiltration. Two different schemes are illustrated schematically in Fig. 2, where the left panel represents the re-infiltration scheme, and the right does not. The CREST-iMAP V 1.0 and V1.1 are openly accessible from https://github.com/chrimerss/CREST-iMAP.

CREST-iMAP inherits the previous version of the CREST model, which simulates saturation excess runoff as the primary runoff generation process (Wang et al., 2011; Xue et al., 2013; Flamig et al., 2020; Li et al., 2022a,b). The schematic model structure is depicted in Fig. 2. The study area is discretized in variable triangular meshes which allow higher density in river channels to resolve high-resolution river flow. Each modeling unit receives excess rainfall (rainfall minus evaporation) from forcing data. Then surface water is divided into overland flow and soil water according to the impervious area ratio through linear weighting. Overland flow is generated once soil water exceeds its holding capacity; otherwise, soil water is separated into the remaining amount and interflow based on the Variable Infiltration Curve (VIC) concept, as shown in Eq. (1). The VIC model is a widely recognized infiltration model that has been applied in several classic hydrologic models (Liang et al., 1994; Zhao, 1995). Overland flow, combined with the impervious area and saturation excess flow, is eventually fed into the 2D shallow water equation solver – the Finite Volume Scheme. It solves water depth and momentum distributed at each grid cell and propagates across boundaries. The outputs of the model include water depth, velocity, discharge, and soil moisture at a desired time step. The flexibility of the unstructured mesh in CREST-iMAP allows dense meshes in regions that reflect high terrain variability (e.g., river channel) and sparse meshes in other regions (e.g., flood plain). This study simulates the extreme flood events at 10-m resolution using the embedded

Table 1
Digital Elevation Model and surveyed channel bottom elevation comparison.

id	lat	lon	gage (feet)	gage (meter)	NED_10m	Difference (m)
1650	29.965025	−95.271954	52.82	16.099536	16.53	−0.430464
1630	29.933648	−95.233574	31.61	9.634728	10.51	−0.875272
1680	29.861698	−95.334883	39.21	11.951208	12.04	−0.088792
1690	29.892682	−95.396717	59.72	18.202656	18.7	−0.497344
1675	29.849306	−95.282843	18	5.4864	5.5	−0.0136
1620	29.837012	−95.233773	−2.12	−0.646176	0.29	−0.936176
1685	29.849798	−95.229007	0.51	0.155448	1.63	−1.474552
1640	29.91791	−95.306565	35.39	10.786872	11.96	−1.173128
1600	29.891907	−95.237623	17.03	5.190744	5.75	−0.559256
1670	29.948972	−95.51941	99.2	30.23616	30.33	−0.09384
1160	29.973483	−95.598483	101.14	30.827472	31.14	−0.312528
1660	29.956166	−95.416142	64	19.5072	20.06	−0.5528
1655	29.972595	−95.435011	76.91	23.442168	23.63	−0.187832

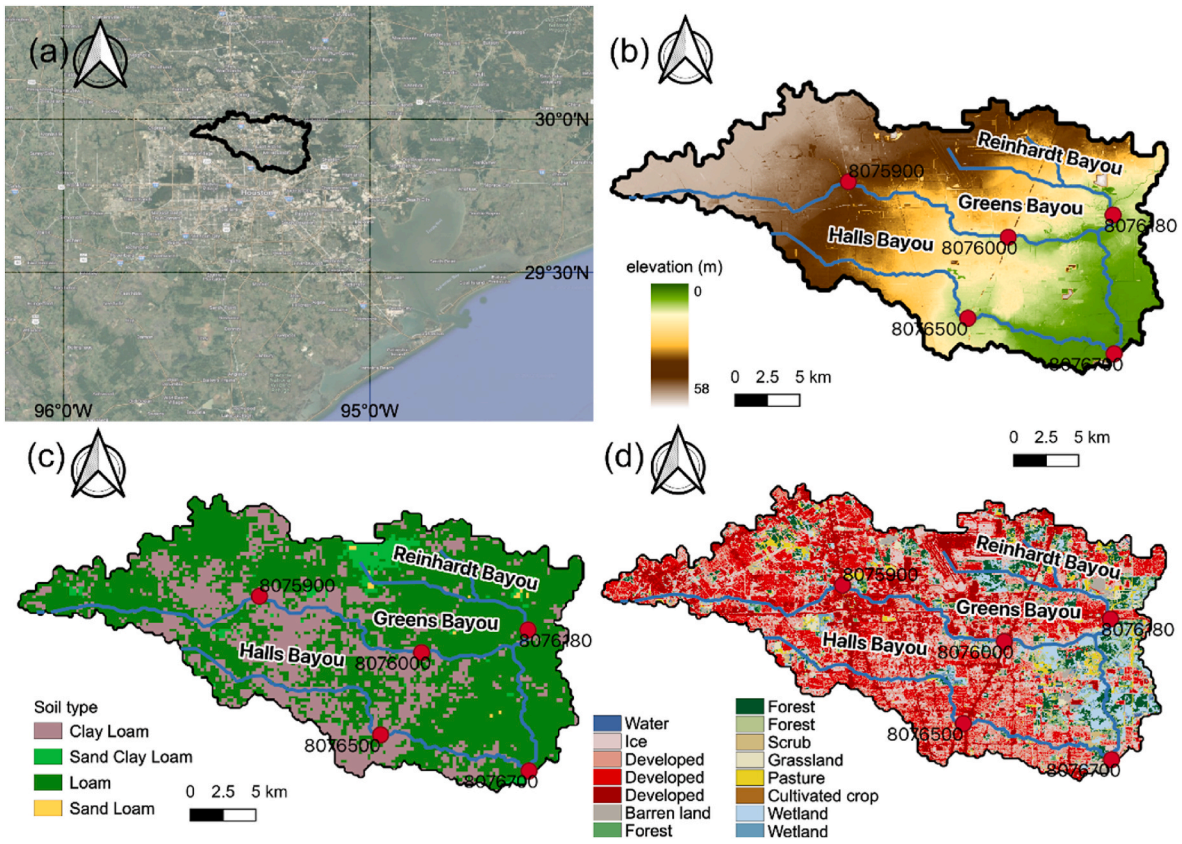

Fig. 1. Maps of the (a) location of the study region, (b) digital elevation model, (c) soil type, and (d) land use land cover.

unstructured mesh generator.

$$i = i_{max} \times \left[1 - (1 - A)^{\frac{1}{B}}\right], \tag{1}$$

where i is the infiltration rates, i_{max} is the maximum infiltration capacity, A is the fractional area of the curve, and B is the exponent of the VIC curve.

There are five hydrologic parameters and one hydraulic parameter for the CREST-iMAP, which are listed in Table 2 along with parameter ranges. It is noteworthy that all these parameters are spatially distributed to account for the spatial heterogeneity of land cover and soil types. The mean soil saturated hydraulic conductivity, *Ksat* f $i = i_{max} \times \left[1 - (1 - A)^{\frac{1}{B}}\right]$, rom 0 to 20 mm/d, indicates the soil infiltration capability. Higher *Ksat* values imply higher infiltration rates if soils are not saturated while reaching plateau for the saturated soils. The mean soil water capacity, *WM* from 10.4 to 365.4 mm, measures the total water content the soil can hold with lower value representing the impermeable soils. The exponent of the Variable Infiltration Curve (VIC), *B*, determines soil water partitioned to saturation excess runoff or interflow, with a higher *B* value corresponding to higher infiltration rates. *KE* is the ratio of the potential evapotranspiration to actual evapotranspiration, similar to the concept of pan coefficient. These soil-related a-priori parameters can be approximated from a look-up table at an individual grid cell basis (Chow et al., 1988). There are also CONUS-wide optimized parameter sets that are configured for operational flood monitoring systems (Flamig et al., 2020). The impervious area ratio, *IM* from 0% to 100%, is obtained directly from the NLCD dataset; the manning's n coefficient is derived from the LULC via a look-up table. Both parameters determine water conveyance capacity, meaning that higher values relate to faster and larger flood peaks. The hydrologic parameters are configured at their optima based on previous study – a CONUS-wise calibrated parameters (Flamig et al., 2020) and shown in Fig. S1, but for the hydraulic parameter – manning coefficient, we manually adjusted it in a preceding event to ensure generating timely and accurate possible flood peaks. Specifically, we use 2017-08-20 to 2017-08-25 to calibrate the manning coefficient, as well as in-channel water stage.

2.5. Experiment

2.5.1. Synthetic experiment

The importance of re-infiltration in principle is governed by (1) soil properties, (2) soil water saturation, and (3) excess rainfall rates. To quantify the relative importance and generalize our results, we decide to conduct a sensitivity test in this study area to mimic different environment while preserving other variables. The sensitivity analysis addresses the following hypotheses: 1) discernible differences exist when switching on and off re-infiltration scheme, 2) re-infiltration alters flood inundation magnitude and dynamics, 3) differences are amplified when increasing soil infiltration rates and drying antecedent soil saturation, and 4) differences increase with more frequent rainfall storms. Of five hydrologic parameters, we select two soil parameters (i.e., *Ksat* and *B*) that have a direct interaction with infiltration rates. Increase in *Ksat* and *B* promote re-infiltration amount. Additionally, the antecedent soil moisture (SM_0) and roughness parameter (n), proven to be critical for flood generation (Li et al., 2021b; Yang et al., 2011), is another term to change infiltration dynamics. We applied a multiplier to each parameter of interest, ranging from 0.0 to 2.0 with 0.1 spacing except for SM_0 that only ranges from 0.0 (completely dry) to 1.0 (fully saturated) with 0.1 spacing. The initial values of parameters are found in Fig. S1.

For the forcing data in this experiment, we consider a 100-year extreme in the study area by looking up the local Intensity-Duration-Frequency table. This determined rainfall rates are uniform across 2 h without spatial heterogeneity to eliminate the impact of rainfall spatial structure because we solely consider the impact by soils. We run the model for 24 h for each parameter, totaling 50 runs.

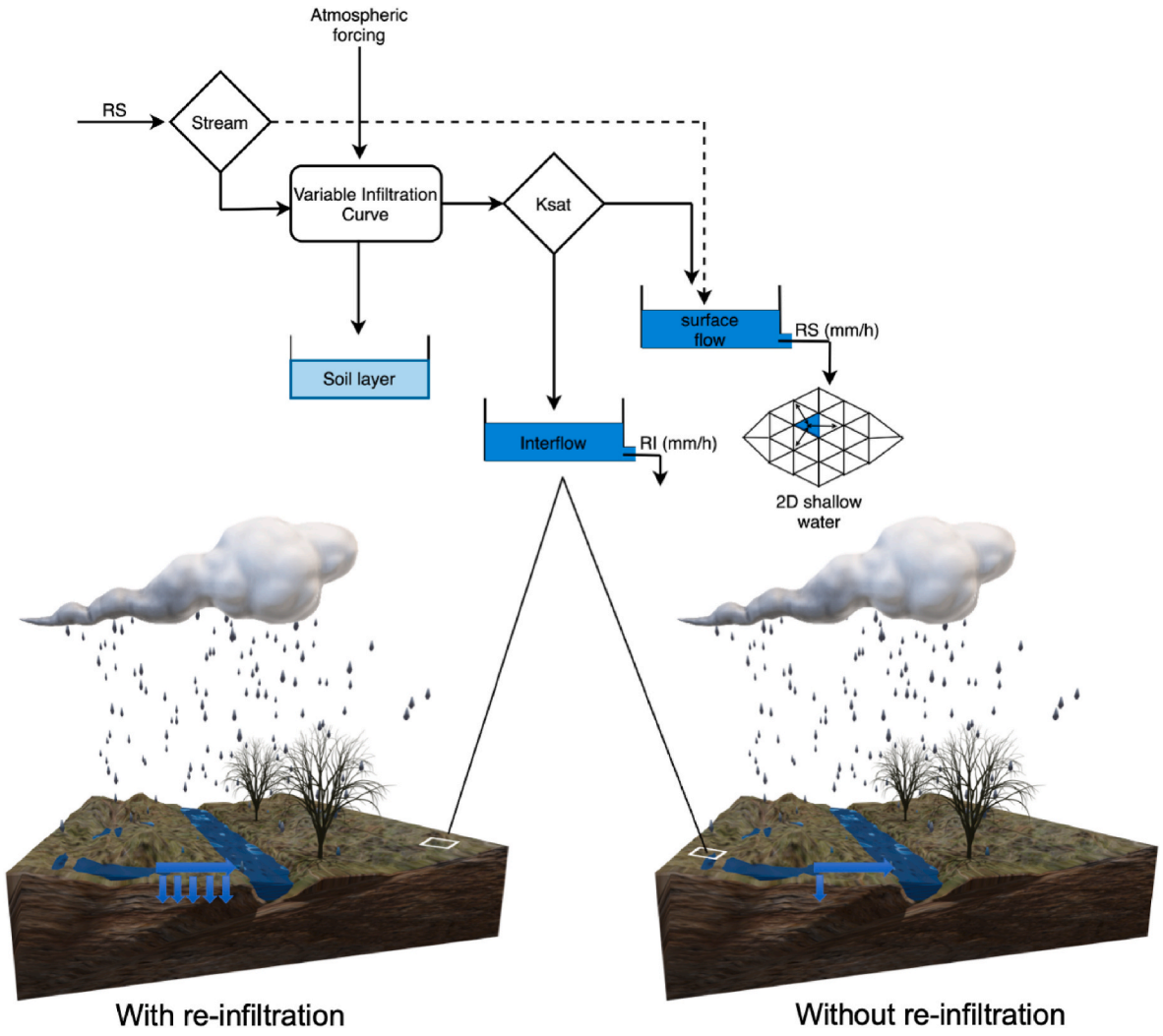

Fig. 2. Schematic illustration of the re-infiltration scheme.

Table 2
Parameters required in CREST-iMAP framework.

Parameters	description	Range
Ksat	Soil saturated hydraulic conductivity (mm/d)	0–2827.2
WM	Mean soil water capacity (mm)	80–200
B	The exponent of the variable infiltration curve	0.05–1.5
IM	Impervious area ratio (%)	0–100
KE	The ratio of the PET to actual evapotranspiration	0.1–1.5
SM_0	Initial soil moisture	0–1
Manning's n	The coefficient for the use of manning's equation in channel flow	0–1

2.5.2. Real case – Hurricane Harvey

Hurricane Harvey is one of the most destructive extreme weather events happened in this study area with substantial damaging winds and urban flooding. The storm was stalled over the Houston region for one week with continuous falling of extreme rains to develop pluvial and fluvial flooding, compounded by costal surges. According to the precipitation estimates by gauges and radars, 1539 mm maximum rainfall was observed, and most locations in the study area recorded at least 760 mm rainfall, making it the wettest tropical cyclone on record. As a result, almost 25–30 percent of Harris Country was submerged during this event, leading to at least $125 billion economic damage, the second largest natural disasters in US history. Many stream gauges malfunctioned (e.g., being flushed) during high flows. Owing to the socioeconomic impact, a variety of flood simulations were conducted in this region (Chen et al., 2021, 2022; Dullo et al., 2021; Li et al., 2021b; Sebastian et al., 2021). The simulation in our study is conducted from 2017-08-26 to 2017-09-01, during which we did not vary model parameters between scenarios with and without re-infiltration. The parameter values are optimized from a previous study (Li et al., 2021b). The initial soil moisture states are obtained from the operational FLASH project (flash.ou.edu/new).

2.6. Computational metrics and results interpretation

A set of computational metrics are selected for this study. The binary assessment comparing the scenarios with and without re-infiltration is considered with Positive Positives (PP), Positive Negatives (PN), and Negative Positives (NP). The first notion indicates whether the model results with re-infiltration detects floods, while the second for model results without re-infiltration scheme. The rationale behind this is that flood extent observations, e.g., witness reports, watermark, satellite-derived flood extent, and insurance claims, are still uncertain without ground truth (Bates, 2004; Chen et al., 2021, 2022). For flood magnitude, the depth, area, and volume are calculated as a basin-integrated ratio. For flood dynamics, we inspect the initial inundation timings and total inundation duration that are often factored in flood risk assessments (Merz et al., 2010). The first six metrics listed in Table 3 are calculated at the maximum flood depth across the simulation period. In

Table 3
Computational metrics used in this study.

Metrics	Formula	Range
Positive Positives (PP)	$\frac{\sum_{n=1}^{N}(B_n=1)\cap(S_n=1)}{N}\times 100\%$	(0, 100) %
Negative Positives (NP)	$\frac{\sum_{n=1}^{N}(B_n=1)\cap(S_n=0)}{N}\times 100\%$	(0, 100) %
Positive Negatives (PN)	$\frac{\sum_{n=1}^{N}(B_n=0)\cap(S_n=1)}{N}\times 100\%$	(0, 100) %
Flood area ratio (R_F)	$R_F=\frac{Area_s}{Area_b}$	(0, 1)
Mean water depth ratio (R_H)	$R_H=\frac{\sum_{i=1}^{n}H_{s,i}}{\sum_{i=1}^{n}H_{b,i}}$	(0, 1)
Surface water volume ratio (R_V)	$R_V=\frac{\sum_{i=1}^{n}H_{s,i}\times Area_s}{\sum_{i=1}^{n}H_{b,i}\times Area_b}$	(0, 1)
Initial inundation time differences (T_{init})	$T_{init}=T_s-T_b$	(-T, +T)
Inundation duration differences (D)	$D=D_s-D_b$	(-T, +T)
Nash- Sutcliffe Efficiency coefficient (NSE)	$1-\frac{\sum_{n=1}^{N}(S_n-O_n)^2}{\sum_{n=1}^{N}(S_n-\overline{O})^2}$	(-inf, 1)
Root Mean Square Error (RMSE)	$\sqrt{\frac{1}{N}\sum_{n=1}^{N}(S_n-O_n)^2}$	(0, inf)
Correlation Coefficient (CC)	$\frac{\sum_{i=1}^{n}(o_i-\overline{o})(s_i-\overline{s})}{\sqrt{\sum_{i=1}^{n}(s_i-\overline{s})^2}\sqrt{\sum_{i=1}^{n}(o_i-\overline{o})^2}}$	(0, 1)

Note: subscript s represents the simulation by turning on the re-infiltration scheme, and subscript b indicates the benchmark that turns off the re-infiltration scheme. T is the total simulation time and O denotes the observed river stage.

the real case study, we verify the performance of two schemes against stream gauge measurements, which is so far the most conventional and trustworthy source. During the verification, the Nash-Sutcliffe Efficiency (NSE) and Correlation Coefficient (CC) are the primary evaluation scores with each indicating the best value of 1. The detailed formulas for calculating these variables are listed in Table 3, as well as their ranges.

The RMSE can be further decomposed to reveal the systematic error and random error (Tang et al., 2020). First, we assume an additive error model by fitting a linear regression to our simulated stage to determine regression coefficients *a* and *b*. We assign the new variable as *F*. Then the residual is calculated by the difference of observed river stage *O* and fitted river stage *F*.

$$F = a \times S + b \tag{2}$$

$$RMSE_S = \sqrt[2]{\frac{1}{n}\sum_{i=1}^{n}(S-F)^2} \tag{3}$$

$$RMSE_R = \sqrt[2]{\frac{1}{n}\sum_{i=1}^{n}(F-O)^2} \tag{4}$$

, where *S* is denoted as the simulated river stage and *O* is the observed.

In the results section, we present it in two parts: sensitivity analysis and real case study. The former includes basin-wise difference in an integral to reveal general differences regarding parameters (Section 3.1.1) and storm intensity (Section 3.1.2). In the real case study, we focus on the efficacy of re-infiltration scheme by comparing to river stage observations (Section 3.2.1), and the High Water Marks surveyed in the aftermath of the event (Section 3.2.2). In Section 3.2.3, we investigate the importance of re-infiltration scheme in real case study by cross-comparing it to the synthetic results.

3. Results

3.1. Sensitivity analysis

3.1.1. Parameter sensitivity

3.1.1.1. Basin-average statistics. The overall flood-related differences between scenarios with and without re-infiltration are shown in Fig. 3, calculated as basin-integral change by averaging each metric over the whole grid cells that are wet (water depth larger than 0.01 m). First, the differences are discernible comparing the two, especially for the surface water volume ratio (R_V), which varies from 0.7 to 1. It suggests the surface water with re-infiltration scheme could only account for 70% of the condition without re-infiltration. Previous studies agree that the re-infiltration results in a substantial reduction of river flow discharge, which can be translated to lower flood depth ratio (R_H) (Nahar et al., 2004; Woolhiser et al., 1996). For different conditions, the antecedent soil moisture, as expected, exhibits the largest impact on flood inundation dynamics when comparing the two scenarios. Lower initial soil moisture leads to greater differences in flood depth ratio (R_H), area ratio (R_F), volume ratio (R_V), and dynamics. For instance, when the initial soil is completely dry, the average flood depth ratio (R_H), area ratio (R_F), and volume ratio (R_V) ratios of the re-infiltration scheme are 85%, 85%, 67%, respectively.

The initial inundation timing for re-infiltration delays around 0.5 h (T_{init}=*0.5*), and the total inundation duration is 2.5 h shorter than the scenario without re-infiltration ($D = 2.5$). The total inundation duration is an important factor for flood risk management (Merz et al., 2010; Triet et al., 2020). As soil gradually approaches saturation, the differences diminish. Saturated hydraulic conductivity, *Ksat*, ranked as the second most sensitive parameter during the test, exponentially reduces flood depth/area/volume by 10%/7%/20% when its multiplier increasing from 0.0 to 2.0. Furthermore, the differences of inundation duration (D) range from 1.5 h to 3.5 h, making *Ksat* the most influential parameter; however, the initial inundation timing is relatively insensitive to it, as opposed to initial soil saturation condition. This is due to the fact that *Ksat* only changes infiltration flux along the way while exerting less impact on the initial inundation timings. For higher surface roughness (n), Flood area ratio (R_F) and volume ratio (R_V) decrease. It is expected because as water flows slowly, more water is accumulated above the surface, leaving higher potential to infiltrate. One exception is for the flood depth ratio (R_H), which increases with roughness. It means differences in water depth are shrinking between two schemes for higher roughness. This implies that with increasing roughness, flood inundation calculated with re-infiltration will result in more concentrated (higher local water depth) yet less widespread (lower inundation areas) flooding. The infiltration parameter *B*, however, has the least impact on the flood inundation dynamics among the three. These measures exhibit the greatest changes at small *B* multipliers (0.1–0.3) and then level out irrespective of increasing *B* multipliers. A plateau is reached because of the constrain of the maximum infiltration capacity. In summary, this sensitivity analysis tests our three main hypotheses, indicating the non-negligible differences between the two schemes and how the soil type and condition influence the results.

3.1.1.2. Spatiotemporal relationships. To explore the spatiotemporal differences of scenarios with and without re-infiltration, we set three parameters to their default values, namely an initially dry soil condition and normal soil infiltration rates (i.e., a-priori setting). Fig. 4 shows the difference in flood extent for the two schemes. Despite a considerable amount of grid cells showing positive agreements (i.e., both detect floods; PP = 16.0%), there are still 1.7% of the grid cells issuing NPs, amounting to 15.6k grid cells (~1.56 km^2) in this model configuration. Specifically, those NPs accumulate around upstream floodplains while the downstream such as areas near the basin outlet does not present

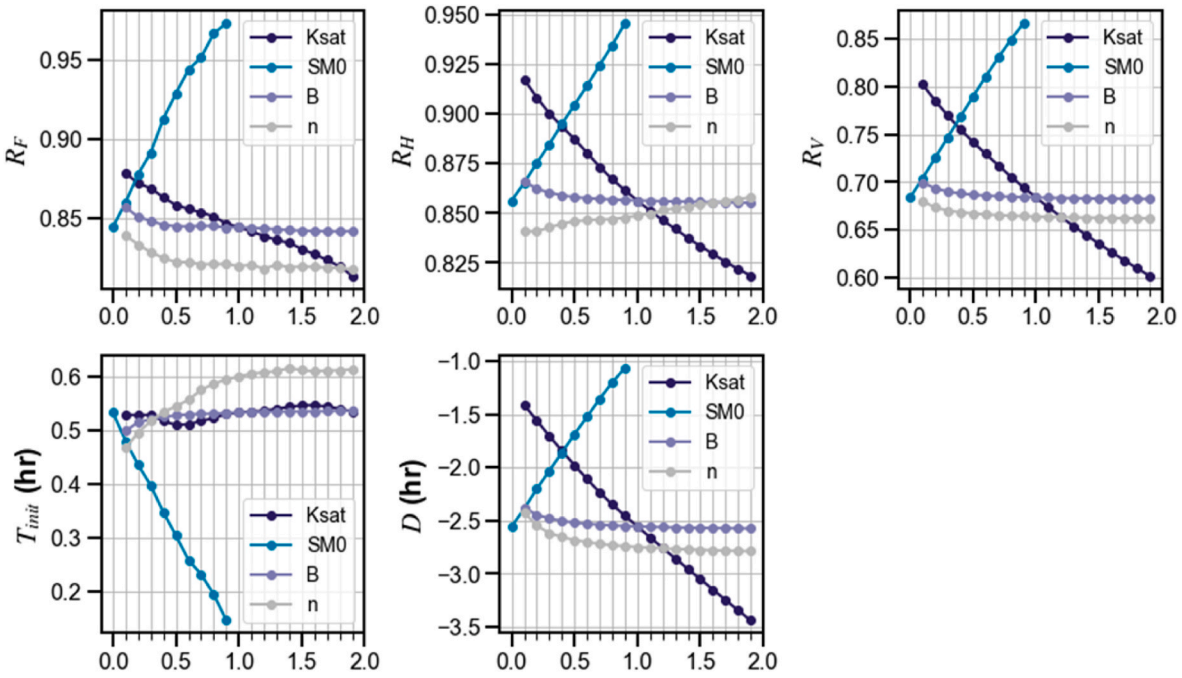

Fig. 3. Plots of parameter sensitivity with metrics indicated in Table 3. R_F: Flood area ratio; R_H: Flood depth ratio; R_V: Water volume ratio; T_{init}: Flood timing differences; D: Flood duration differences. The no-difference point should be located at (1.0,1.0) for R_F, R_H, R_V and (1.0,0.0) for T_{init} and D.

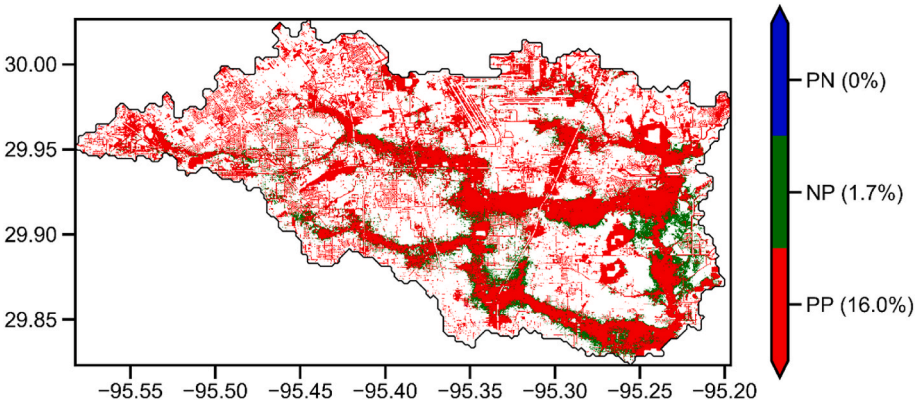

Fig. 4. Map of binary flood detection comparison. PP: Positive Positives; PN: Positive Negatives; NP: Negative Positives.

discernible differences, as the flood depth there due to accumulation is not sensitive to inundation thresholds for flooded cells. Moreover, Fig. 5 portrays the spatial distribution of the differences with respect to maximum depth, initial inundation timings, and total inundation duration. Fig. 5a depicts the major differences that are situated in floodplains and river channels where surface water is accumulated via routing, and the maximum depth difference is up to 3 m in the river channel, especially downstream of Halls Bayou. However, the initial inundation timings and durations are scattered sparsely over the study area, with a majority of the grid cells showing earlier and longer inundations for the case without re-infiltration scenario. Therefore, it is likely that the flood is over-predicted by models without the re-infiltration scenario.

Meanwhile, we notice that there are some samples in the opposite distribution, indicating delayed and/or shorter inundation time (Fig. 5). Arguably, this could be some local effects when the soil reaches earlier saturation in the re-infiltration scenario, thereby leading to earlier flooding. A supporting material is found in Fig. 5d, in which the basin-average soil moistures of two schemes are compared. Notably, evapotranspiration is not considered in this ideal test, so the soil moisture does not deplete with time. During the storm lifetime, soil moisture surges from completely dry to 85% saturation for the scenario without re-infiltration and to 95% saturation for scenario with re-infiltration. Early saturation reduces infiltration rates later on and thus has pronounced effects on local flooding when surface water is not routed timely. Fig. 5e presents the evolution of surface water volume by integrating surface water depth along with grid cells. Although both scenarios concurrently reach the maximum surface water volume, their recession limbs show considerable differences. The re-infiltration scenario apparently has a steep exponential decay, as both still water and running water infiltrates into the soil; for the scenario without re-infiltration, in contrast, there is a mild decay and even levels out at the end of the simulation. The difference between the two increases with time, as shown in the shaded area, up to 0.4×10^8 m^3 volume difference, which equates to almost half of the total surface water volume.

In summary, re-infiltration scheme indeed influences flood magnitude and timings via surface water-soil interaction, and it possibly reduces flood magnitude and delays (shortens) flood timing (duration). Flood magnitude differences are pronounced downstream or in depressions, while flood timings are scattered. Such results are markedly

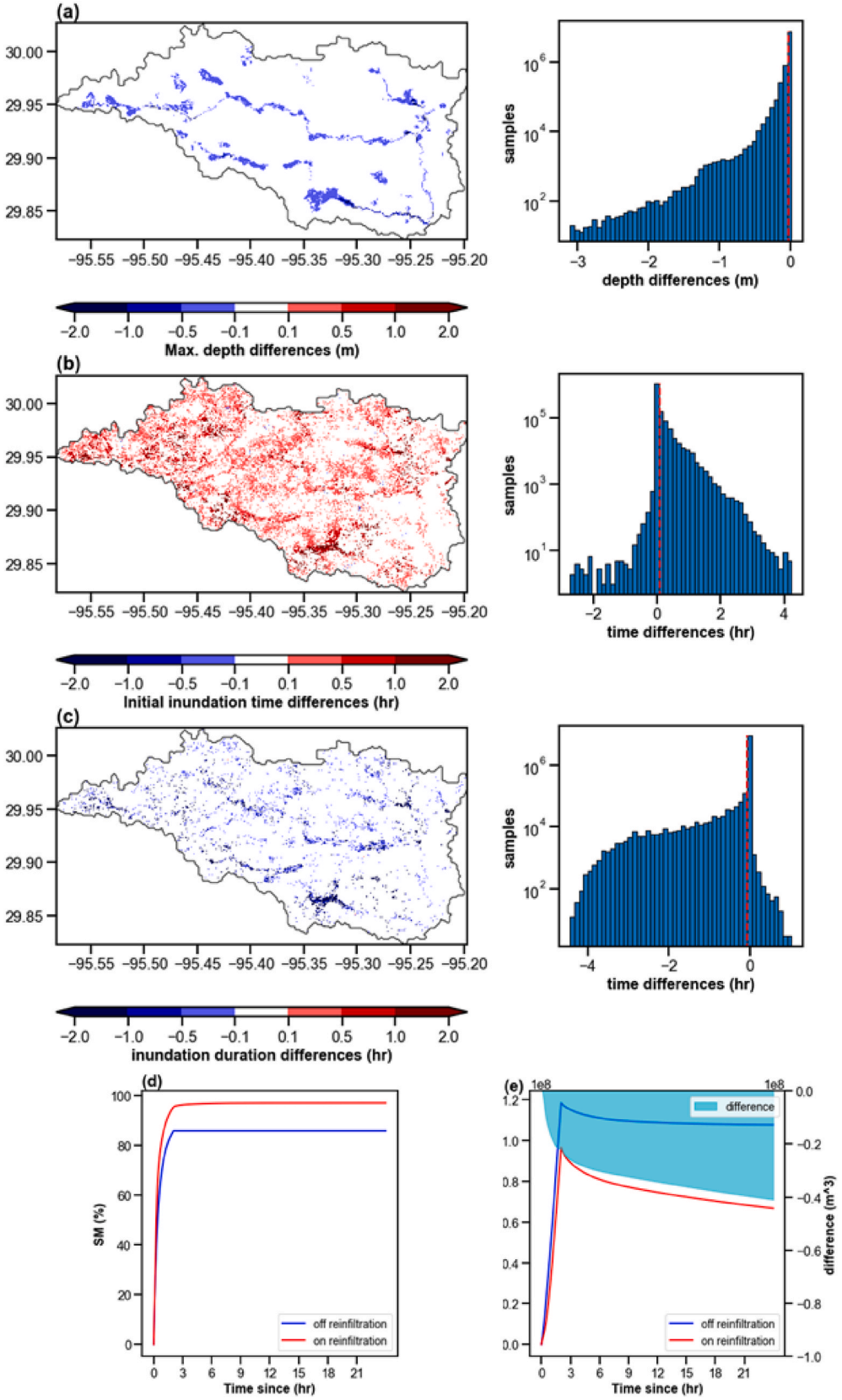

Fig. 5. Spatial distribution of differences of (a) maximum depth, (b) initial inundation timings, and (c) inundation durations along with respective sample distributions (red line represents the mean value of the distribution). Temporal evolution of (d) soil moisture (%) and (e) surface water volume. The difference of surface water volume in (e) is plotted in the shaded area.

tied to soil condition (wet or dry) and soil characteristics (infiltration capacity).

3.1.2. Sensitivity to storm frequency

For less intense storms yet more frequent, the impact of re-infiltration is expected to be larger than more intense storms, as rainfall rates are less likely to exceed infiltration capacity. We looked up 1-year, 2-year, 5-year, 10-year, 25-year, 50-year, and 100-year event rainfall from the NOAA Atlas 14 IDF curve and simulated those events collectively with default parameters. As shown in Fig. 6, three flood magnitude-related metrics (i.e., R_F, R_H, and R_V) verify our speculation. For the 1-year storm specifically, flood areas with re-infiltration only account for 30% of that without re-infiltration. Likewise, flood depth and surface water volumes are reduced by 50% and 75%, respectively. However, there is no monotonic trend for flood timing. Floods are delayed for all storms, but the delayed time increases with return periods prior to peaking at 0.83 h for 10-year storm, after which it decreases. The flood duration differences again decrease with return periods.

3.2. Case study: Hurricane Harvey

The previous sensitivity test indicates that the re-infiltration scheme is not only physically sound, but it exerts considerable influences on model simulations. Although the CREST-iMAP tested under theoretical scenarios, it is relevant to compare one another in a real case study against observations during Hurricane Harvey.

3.2.1. Verification against stream gauges

Gauged water heights from five USGS stream gauges within the model domain are retrieved during model simulations at the 15-min interval. Surface water levels from two simulation schemes are extracted at collocated stream gauge locations. It is worth mentioning that the terrain elevation imposes great uncertainties when comparing model simulations to observations, as the sub-grid variation cannot be resolved in the current settings. Despite the resolution mismatch, these gauge readings are still the most widely used source to verify the model performance. Table 4 shows the respective performance for with and without re-infiltration scenarios with respect to observations. The re-infiltration scheme greatly improves the NSE scores (+139.9%) and CC (+7.24%) while reducing RMSE (−18.2%). Especially for the gauge 08075900, there is more than a 400% increase in NSE score, jumping from 0.12 to 0.69. By breaking down the RMSE into systematic error $RMSE_S$ and random error $RMSE_R$, we see the reduced errors are largely attributed to systematic error (−31.2%), relative to the random error (−13.1%). Thus, the systematic bias is much alleviated by considering the re-infiltration scheme.

The reason for such a performance leap comes from better characterization of its flow recession limbs, as shown in Fig. 7. Both schemes are capable of simulating the peak water height values without delays, but water in the scenario without re-infiltration falls mildly in the recession stage, resulting in much higher water level than the observations. On the other hand, flow for the re-infiltration scenario follows the gauge readings closely, especially after the first peak (from 2017-08-26 to 2017-08-27). Apart from this best-performing gauge, the re-infiltration scheme improves capturing falling water across all the gauge stations, thereby leading to significant performance gains. Consistently, previous studies also highlighted that the re-infiltration markedly reduces recession limbs in the hydrograph (Nahar et al., 2004).

To be noted, water heights during flood recession period are both overestimated by two schemes, pointing to a systematic error in our CREST-iMAP framework. First, the model is calibrated to capture the peaking water height while ignoring the recession period. Second, surface runoff generated by the water balance model has been found to overestimate (Li et al., 2022b). Third, missing model physics such as subsurface exfiltration to channels and manmade structures complicate results interpretation.

3.2.2. Verification against high water marks

Because a direct assessment for flood inundation is not feasible, some watermarks or stains in the aftermath of a flood event can be used as proxy data for model evaluation although with great uncertainties. The USGS team routinely publishes their surveyed High Water Marks

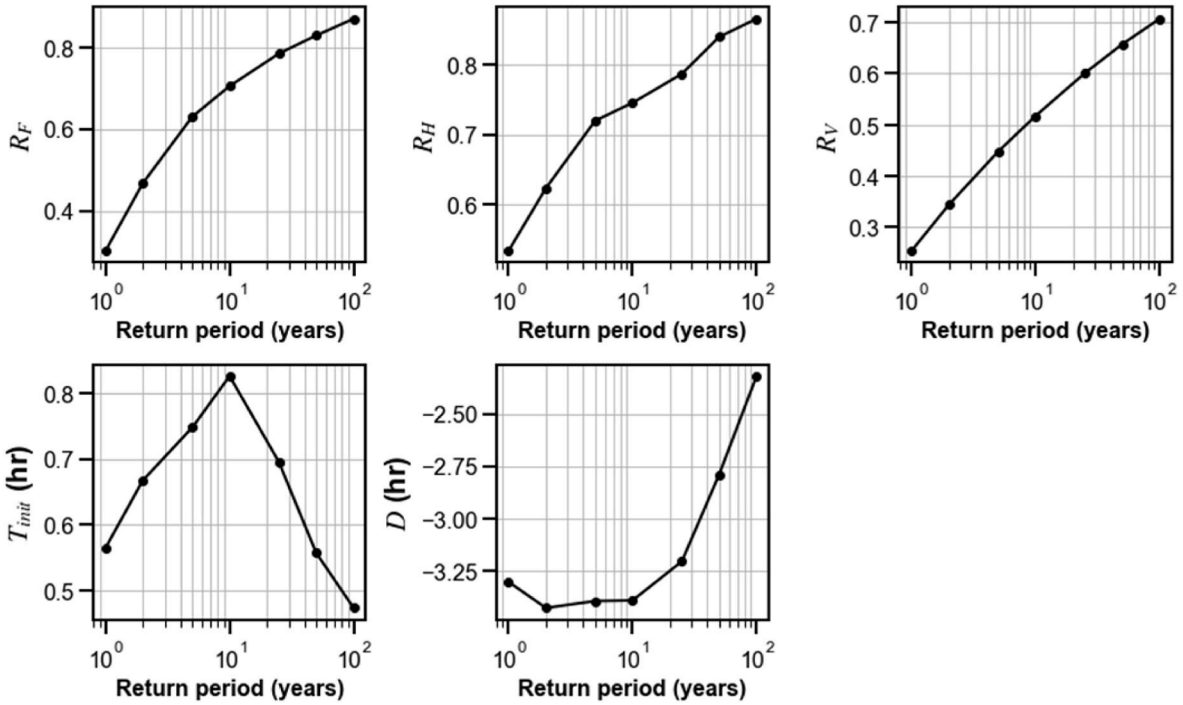

Fig. 6. Similar to Fig. 4, but for storms at different frequencies.

Table 4
Model performance at stream gauge locations. The bolded values are the better ones from the off and on re-infiltration comparison. "Off" represents scenario without re-infiltration and "On" represents with re-infiltration scenario. NSE: Nash-Sutcliffe Coefficient; RMSE: Root Mean Squared Error; CC: Correlation Coefficient.

Metrics\Gauges		08075900	08076000	08076180	08076500	08076700
NSE	Off	0.12	0.20	0.47	0.34	0.921
	On	0.69	0.44	0.52	0.66	0.919
	Improvement (%)	+475	+120	+10.6	+94.1	+0.2
RMSE (m)	Off	1.89	2.24	1.85	1.61	1.14
	On	1.13	1.89	1.76	1.15	1.12
	Improvement (%)	−40.2	−15.6	−4.86	−28.6	−1.8
$RMSE_S$ (m)	Off	1.64	1.39	0.44	1.02	0.96
	On	1.00	1.02	0.26	0.59	0.89
	Improvement (%)	−39.0	−26.6	−40.9	−42.2	−7.3
$RMSE_R$ (m)	Off	0.94	1.77	1.80	1.25	0.61
	On	0.53	1.58	1.74	0.99	0.69
	Improvement (%)	−43.6	−10.7	−3.33	−20.8	+13.1
CC	Off	0.88	0.71	0.70	0.77	0.99
	On	0.96	0.78	0.73	0.87	0.99
	Improvement (%)	+9.09	+9.86	+4.29	+13.0	0

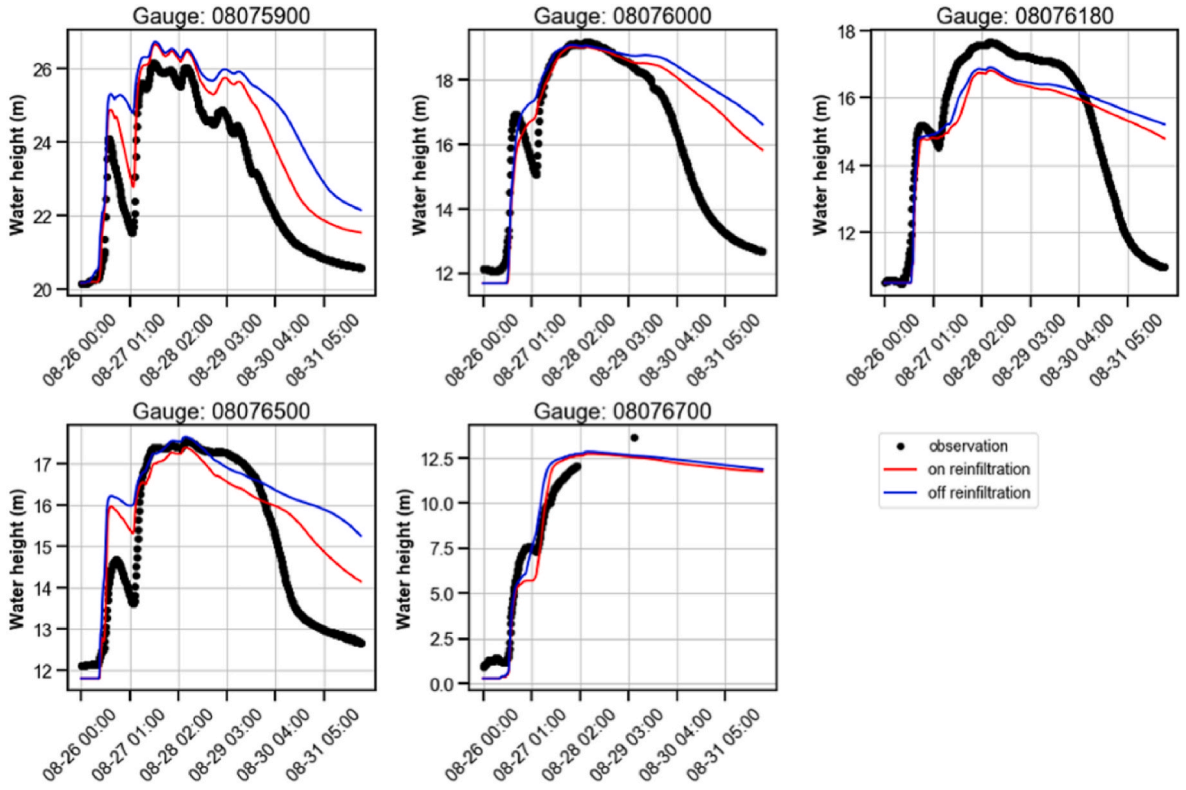

Fig. 7. Simulated and observed time series of surface water level at five USGS stream gauges.

(HWMs) after some major flood events, which can subsequently be used for model evaluations (Chen et al., 2021; Li et al., 2021b; Sebastian et al., 2021; Wing et al., 2017). Fig. 8 shows the cell-wise maximum flood depth of the two schemes compared to the HWMs. Both schemes present better performance upstream of Halls Bayou, with a difference smaller than 0.5 m. However, the model over-predicts water depth in Greens Bayou up to 1.5 m. This is consistent with the over-prediction of in-channel water level, as shown in Fig. 7. The distribution of the differences is shown in Fig. 8c, pointing to a generally better performance of the re-infiltration scenario than without it, as the absolute mean depth difference of the re-infiltration (0.51 m) is 17.2% smaller than that of the scenario without re-infiltration (0.60 m). It is worth noting that HWMs themselves come with uncertainties that are due to the data quality, and errors could be up to 0.2 m (Koenig et al., 2016). For instance, tranquil water represents a smooth trend that has small uncertainties. There are also spurious errors that are related to human mistakes or values being rounded off. This is particularly true for the recorded geographical coordinates which requires more floating points to pin down the location exactly. In Fig. 8d and e, the two HWMs are marked with an absolute difference greater than 1 m but only several pixels away (i.e., tens of meters) from their true values. Despite this, the re-infiltration greatly alleviates the over-prediction of the previous model.

3.2.3. *Intercomparisons of flood magnitude and dynamics during Hurricane Harvey*

The intercomparison of flood magnitude and dynamics helps to understand the effects of re-infiltration in a real 500-year event. Fig. 9, similar to Fig. 5, depicts the basin-integrated differences. For flood dynamics, the initial inundation timing (T_{init}) and total inundation duration (D) could vary from −2 (delayed) to 4 (earlier) hours and 0–15 h, respectively. For the temporal evolution of the Harvey event, it is featured by two subsequent events. The first event from 2017-08-26 to

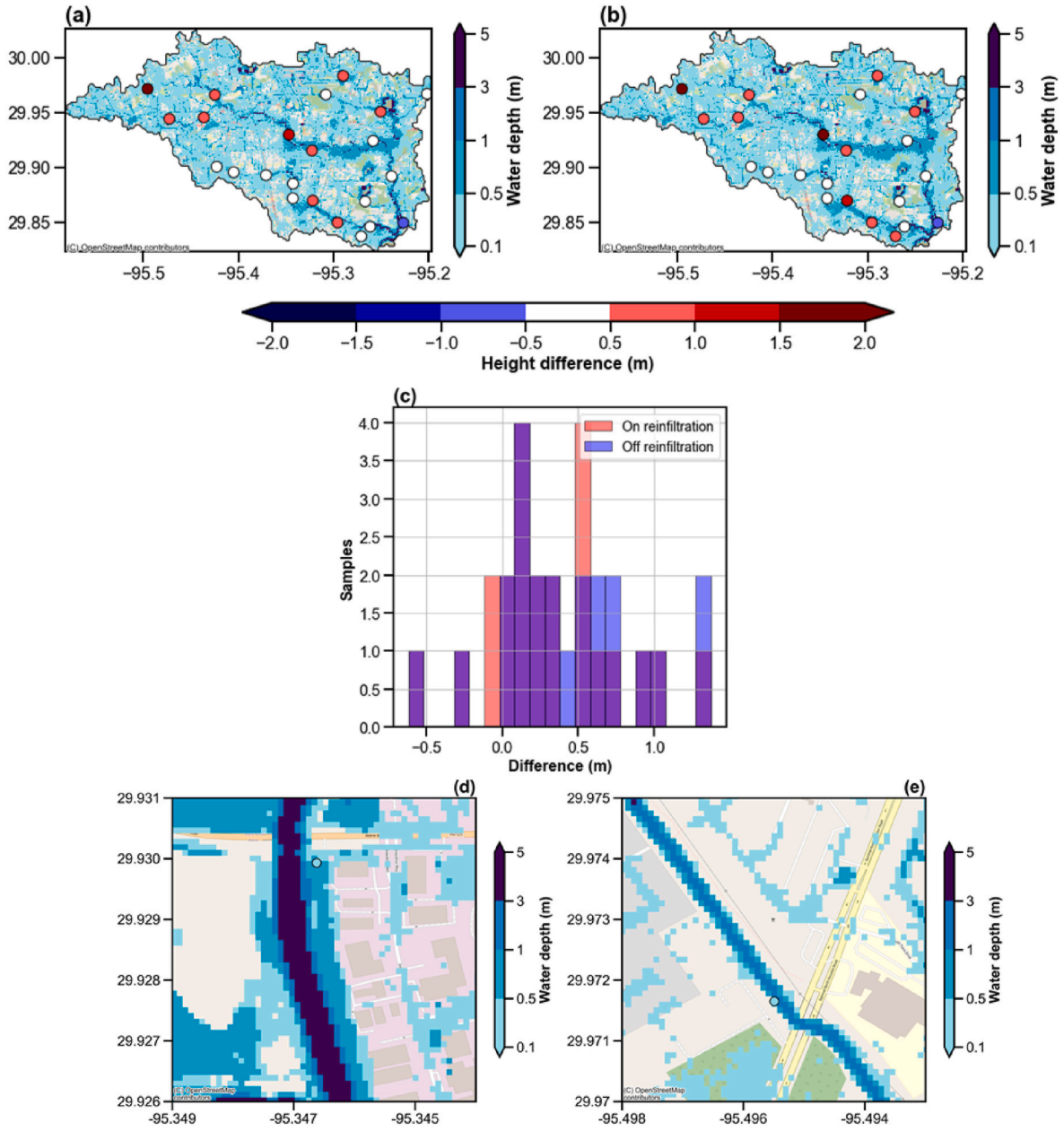

Fig. 8. Maps of maximum surface water depth for (a) on re-infiltration and (b) off re-infiltration with differences against High Water Marks (HWMs). (c) histogram of water depth difference. Maps of two USGS high water marks (d) and (e), with the difference larger than 1 m between the simulation and recorded.

2017-08-27 saturates the soils immediately, during which the large differences of surface water volume and soil moisture are present between the two schemes. The soil moisture content for the re-infiltration scheme is about 10% more than without the re-infiltration scheme; the surface water volume, however, is 40% less. The second event does not produce a large difference because of the saturated soils over the domain (Fig. 9d). As indicated by the sensitivity analysis, this effect is highly dependent on soil condition, soil types, and rainfall characteristics. The extreme rainfall from Harvey leaves less room for water to infiltrate, compared to other less intense events. It is therefore expected to have more pronounced improvements for less intense rainfall or other regions with high soil infiltration capacity.

4. Discussion

In this study, only local variations of four parameters – initial soil moisture, manning's roughness, hydraulic conductivity, and the exponent of the VIC model – are tested independently. However, the interactions among these parameters are not explored herein. Global sensitivity analysis, such as the Morris method used in the previous study (Li et al., 2021b), can measure the variation of each parameter relative to other parameters, so it provides a clearer picture of the parameter interactions. Needless to say, initial soil saturation state is the dominant controller for the differences between the simulations with and without re-infiltration process. When the soils are fully saturated, the with and without re-infiltration scenarios are almost identical if other parameters are the same. Combined with our previous study that underlies the importance of infiltration and initial soil moisture for flood inundation modeling, we highly recommend taking into consideration the initial soil moisture state, as it has not been well-recognized in the hydraulic model community. This can be achieved via three ways: 1) warm up the model for a relatively long period prior to the simulation period (Chen et al., 2020); 2) parameterize the initial soil moisture and calibrate it, similar to the way we treat initial in-channel water depth

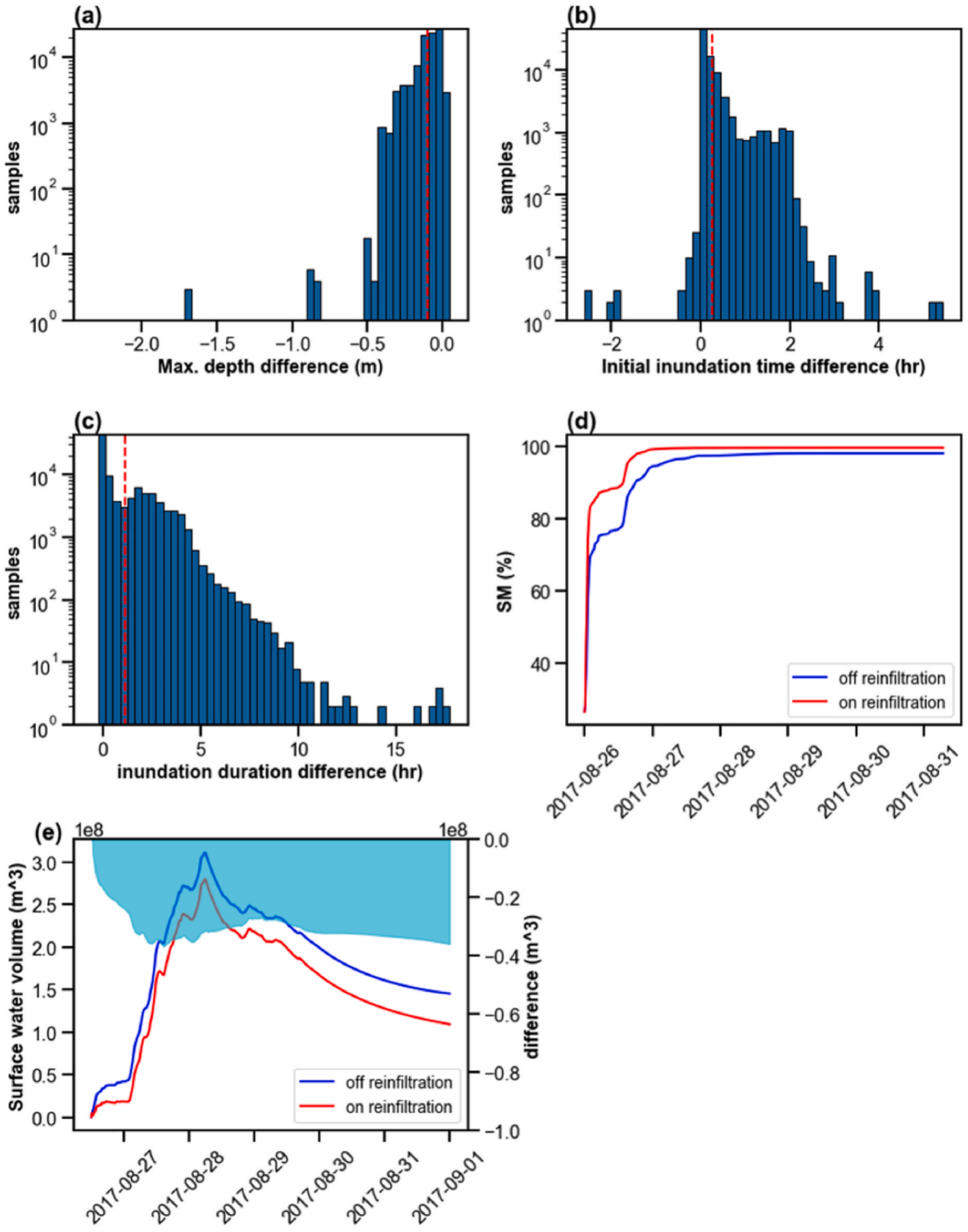

Fig. 9. Basin aggregated distribution of (a) maximum depth differences, (b) initial inundation timing differences, and (c) inundation duration differences averaged over the simulation period. Time series of basin-average (a) soil moisture and (b) surface water volume. The vertical dashed line indicates the mean value of all samples.

(Xue et al., 2013); 3) approximate it using observations or other model simulations, like what has been done in the real case study in Section 3.2 (Flamig et al., 2020). The first approach is ideal because it eliminates uncertainties in parameterization (such as equifinality) or error propagation from observations/simulations to models; it is, however, the most computationally expensive approach for hydraulic modeling compared to the other two. Approach two and three are more pragmatic, while both inherit uncertainties or errors. We prefer the third approach if the data source is found to be trustworthy. For instance, in our case study, we used the simulated soil moisture product from the operational CREST/EF5 model which shares the same land surface processes as the CREST-iMAP.

The results relating to different rainfall events are considered in this study (i.e., 1-year, 2-year, 5-year, 10-year, 25-year, 50-year, and 100-

year rainfall). As for lower storm intensity, the differences between the two schemes enlarge, as rainfall rates are less likely to exceed the infiltration capacity, and soils are not saturated. Other environmental factors pertaining to different topography and physiography are also likely to interact and change the results. For instance, an increase in slope will leave less room for surface water to re-infiltrate, which explains why re-infiltration compromises its importance in hillslope hydrology (Corradini et al., 2002; Zhang et al., 2020).

5. Conclusions

This study focuses on the influence of the re-infiltration process for 100-year and 500-year flood events, which has so far not been well-recognized by the hydrologic/hydraulic modeling community. The sensitivity experiment and a 500-year Hurricane Harvey example both highlight the discernible differences between the with and without re-infiltration scheme. The major conclusions are summarized as follows:

1. In the 100-year design rainfall event, re-infiltration is found to make discernible differences with less flood extent (~1.56 km^2), depth (~3 m), and dynamics (~4-h delayed flooding and ~4-h shorter inundation duration), compared to without re-infiltration. The differences are increasing with more frequent storms. The 500-year Hurricane Harvey event shows a magnified difference in inundation duration up to 15 h because of the longer event duration. However, the flood depth difference is less in the Harvey event due to the rapid saturation of the soils.
2. The hydraulic conductivity and antecedent soil condition from the designed sensitivity test are found to be the prime contributors to the difference between with and without re-infiltration, and comparatively, the antecedent soil moisture condition is the most sensitive among the four tested factors.
3. For the Harvey event, the differences are verified with stream gauge observations. On average, a 139.9% increase in NSE scores is found for re-infiltration with respect to without it. The improvements are mostly tied to better characterization of the recession limb after peak flow while the peak flows are well-captured by both. The proxy data – USGS High Water Marks – also indicate better performance with the inclusion of the re-infiltration scheme, as the re-infiltration scheme presents a 17.2% less flood depth difference than the case without the re-infiltration. The differences are further expected to enlarge for less intensive events and regions with a higher percentage of permeable soil media.

This study aims to raise attention to the important re-infiltration process in coupled H&H flood modeling to provide more accurate flood information, e.g., depth and timings. For future work, we will continue improving the current CREST-iMAP model framework by incorporating flood mitigation measures such as levees and dams into the system. Also, it is critical to couple with the NWP model to advance flood prediction lead time, which ensures more time for residents at risk to evacuate.

Software availability

Software name: CREST-iMAP Version 1.1.

Programing language: Python and C

The main package is developed using the Python language version 2.7. Some bottlenecks that are computationally expensive (e.g., hydrologic component and mesh generator) are written and compiled in C language for efficiency. It has been tested both on Linux and MacOS operating systems. Both CREST-iMAP Version 1.0 (without re-infiltration) and 1.1 (with re-infiltration) can be accessed from the HydroShare: http://www.hydroshare.org/resource/50ce0d7d80b642898f74d8bf56798565.

Declaration of competing interest

The authors declare that they have no known competing financial interests or personal relationships that could have appeared to influence the work reported in this paper.

Acknowledgements

The first author is partially sponsored by the University of Oklahoma Hydrology and Water Security Program, the National Science Foundation PIRE Project, and the Graduate College Hoving Fellowship. The authors would like to thank the forcing data and validation data providers – the National Oceanic and Atmospheric Administration National Severe Storms Laboratory team and the Unites States Geological Survey.

Appendix A. Supplementary data

Supplementary data to this article can be found online at https://doi.org/10.1016/j.envsoft.2022.105450.

References

Allen, R.G., Pereira, L., Raes, D., Smith, M., 1998. Crop Evapotranspiration, Food and Agriculture Organization of the United Nations, vol. 56. FAO publication, Rome, Italy, p. 290. ISBN 92-5-104219-5.

Bravo, J.M., Allasia, D., Paz, A.R., Collischonn, W., 2012. Coupled hydrologic-hydraulic modeling of the upper Paraguay river basin. J. Hydrol. Eng. 17, 635–646. https://doi.org/10.1061/(ASCE)HE.1943-5584.0000494.

Bates, P., 2004. Remote sensing and flood inundation modelling. Hydrol. Process. 18, 2593–2597.

Bates, P.D., Quinn, N., Sampson, C., Smith, A., Wing, O., Sosa, J., et al., 2021. Combined modeling of US fluvial, pluvial, and coastal flood hazard under current and future climates. Water Resour. Res. 57 https://doi.org/10.1029/2020WR028673 e2020WR028673.

Berghuijs, W.R., Woods, R.A., Hutton, C.J., Sivapalan, M., 2016. Dominant flood generating mechanisms across the United States. Geophys. Res. Lett. 43, 4382–4390. https://doi.org/10.1002/2016GL068070.

Buchanan, B., Auerbach, D.A., Knighton, J., Evensen, D., Fuka, D.R., Easton, Z., et al., 2018. Estimating dominant runoff modes across the conterminous United States. Hydrol. Process. 32, 3881–3890. https://doi.org/10.1002/hyp.13296.

Chen, M., Nabih, S., Brauer, N.S., Gao, S., Gourley, J.J., Hong, Z., et al., 2020. Can remote sensing technologies capture the extreme precipitation event and its cascading hydrological response? A case study of hurricane Harvey using EF5 modeling framework. Rem. Sens. 12, 445. https://doi.org/10.3390/rs12030445.

Chen, M., Li, Z., Gao, S., Luo, X., Wing, O.E., Shen, X., et al., 2021. A comprehensive flood inundation mapping for hurricane Harvey using an integrated hydrological and hydraulic model. J. Hydrometeorol. 22, 1713–1726.

Chen, M., Li, Z., Gao, S., 2022. Multisensor remote sensing and the multidimensional modeling of extreme flood events. In: Zhang, K., Hong, Y., AghaKouchak, A. (Eds.), Remote Sensing of Water-Related Hazards. https://doi.org/10.1002/9781119159131.ch5.

Chow, V.T., Maidment, D.R., Mays, L.W., 1988. Applied Hydrology. *McGraw-Hill Series in Water Resources and Environmental Engineering*, McGraw-Hill, Inc., New York.

Cohen, S., Praskievicz, S., Maidment, D.R., 2018. Featured collection introduction: National water model. J. Am. Water Resour. Assoc. 54 (4), 767–769. https://doi.org/10.1111/1752-1688.12664.

Corradini, C., Morbidelli, R., Melone, F., 1998. On the interaction between infiltration and Hortonian runoff. J. Hydrol. 204, 52–67.

Corradini, C., Govindaraju, R.S., Morbidelli, R., 2002. Simplified modelling of areal average infiltration at the hillslope scale. Hydrol. Process. 16, 1757–1770.

Dullo, T.T., Ganguade, S., Morales-Hernandez, M., Sharif, M.B., Kao, S.C., Kalyanapu, A. J., et al., 2021. Simulation of Hurricane Harvey flood event through coupled hydrologic-hydraulic models: challenges and nex steps. Journal of Flood Risk Management 14, 1–26. https://doi.org/10.1111/jfr3.12716.

Felder, G., Zischg, A., Weingartner, R., 2017. The effect of coupling hydrologic and hydrodynamic models on probable maximum flood estimation. J. Hydrol. 550, 157–165. https://doi.org/10.1016/j.jhydrol.2017.04.052.

Flamig, Z.L., Vergara, H., Gourley, J.J., 2020. The ensemble framework for flash flood forecasting (EF5) v1.2: description and case study. Geosci. Model Dev. 13, 4943–4958. https://doi.org/10.5194/gmd-13-4943-2020.

Gourley, J.J., Flamig, Z.L., Vergara, H., Kirstetter, P., Clark, R.A., Argyle, E., et al., 2017. The FLASH project: improving the tools for flash flood monitoring and prediction across the United States. Bull. Am. Meteorol. Soc. 98, 361–372. https://doi.org/10.1175/BAMS-D-15-00247.1.

Getirana, A.C.V., Paiva, R.C.D., 2013. Mapping large-scale river flow hydraulics in the Amazon basin. Water Resour. Res. 49, 2437–2445. https://doi.org/10.1002/wrcr.20212.

Grimaldi, S., Schumann, G.J.-P., Shokri, A., Walker, J.P., Pauwels, V.R.N., 2019. Challenges, opportunities and pitfalls for global coupled hydrologic-hydraulic modeling of floods. Water Resour. Res. 55, 5277–5300. https://doi.org/10.1029/2018WR024289.

Hirabayashi, Y., Mahendran, R., Koirala, S., Konoshima, L., Yamazaki, D., Watanabe, S., et al., 2013. Global flood risk under climate change. Nat. Clim. Change 3 (9), 816–821.

Johnson, J.M., Munasinghe, D., Eyelade, D., Cohen, S., 2019. An integrated evaluation of the National Water Model (NWM)-Height above Nearest Drainage (HAND) flood mapping methodology. Nat. Hazards Earth Syst. Sci. 19, 2405–2420. https://doi.org/10.5194/nhess-19-2405-2019.

Kenward, T., Lettenmaier, D.P., Wood, E.F., Fielding, E., 2000. Effects of digital elevation model accuracy on hydrologic predictions. Rem. Sens. Environ. 74 (3), 432–444. https://doi.org/10.1016/S0034-4257(00)00136-X.

Kim, J., Warnock, A., Ivanov, V.Y., Katopodes, N.D., 2012. Coupled modeling of hydrologic and hydrodynamic processes including overland and channel flow. Adv. Water Resour. 37, 104–126. https://doi.org/10.1016/j.advwatres.2011.11.009.

Koenig, T.A., Bruce, J.L., O'Connor, J.E., McGee, B.D., Holmes Jr., R.R., Hollins, Ryan, Forbes, B.T., et al., 2016. Identifying and preserving high-water mark data: U.S. Geological Survey Techniques and Methods, book 3, 47. https://doi.org/10.3133/tm3A24 chap. A24.

Li, Z., Chen, M., Gao, S., Hong, Z., Tang, G., Wen, Y., Hong, Y., 2020. Cross-examination of similarity, difference and deficiency of gauge, radar and satellite precipitation measuring uncertainties for extreme events using conventional metrics and multiplicative triple collocation. Rem. Sens. 12, 1258. https://doi.org/10.3390/rs12081258.

Li, Z., Chen, M., Gao, S., Gourley, J.J., Yang, T., Shen, X., et al., 2021a. A multi-source 120-year U.S. flood database with a unified common format and public access. Earth Syst. Sci. Data 13, 3755–3766. https://doi.org/10.5194/essd-2021-36.

Li, Z., Chen, M., Gao, S., Luo, X., Gourley, J.J., Kirstetter, P., et al., 2021b. CREST-iMAP v1.0: a fully coupled hydrologic-hydraulic modeling framework dedicated to flood inundation mapping and prediction. Environ. Model. Software 141, 105051. https://doi.org/10.1016/j.envsoft.2021.105051.

Li, Z., Gao, S., Chen, M., Gourley, J.J., Liu, C., Prein, A., Hong, Y., 2022a. The conterminous United States are projected to become more prone to flash floods in a high-end emissions scenario. Commun. Earth Environ. 3, 86. https://doi.org/10.1038/s43247-022-00409-6.

Li, Z., Gao, S., Chen, M., Gourley, J., Mizukami, N., Hong, Y., 2022b. CREST-VEC: a framework towards more accurate and realistic flood simulation across scales [preprint] Geosci. Model Dev. Discuss. (GMDD). https://doi.org/10.5194/gmd-2022-61. submitted for publication).

Liang, X., Lettenmaier, D.P., Wood, E.F., Burges, S.J., 1994. A simple hydrologically based model of land surface water and energy fluxes for general circulation models. J. Geophys. Res., [Atmos.] 99, 14415–14428. https://doi.org/10.1029/94JD00483.

Mahapatra, S., Jha, M.K., Biswal, S., Senapati, 2020. Assessing variability of infiltration characteristics and reliability of infiltration models in a tropical sub-humid region of India. Sci. Rep. 10, 1515. https://doi.org/10.1038/s41598-020-58333-8.

Merz, B., Kreibich, H., Schwarze, R., Thieken, A., 2010. Review article "Assessment of economic flood damage. Nat. Hazards Earth Syst. Sci. 10, 1697–1724. https://doi.org/10.5194/nhess-10-1697-2010, 2010.

Mohanty, P.M., Nithya, S., Nair, A.S., Indu, J., Ghosh, S., Bhatt, C.M., et al., 2020. Sensitivity of various topographic data in flood management: implications on inundation mapping over large data-scarce regions. J. Hydrol. 590, 125523 https://doi.org/10.1016/j.jhydrol.2020.125523.

Nahar, N., Govindaraju, R.S., Corradini, C., Morbidelli, R., 2004. Role of run-on for describing field-scale infiltration and overland flow over spatially variable soils. J. Hydrol. 286, 36–52. https://doi.org/10.1016/j.jhydrol.2003.09.011.

Nguyen, P., Thorstensen, A., Sorooshian, S., Hsu, K., AghaKouchak, A., Sanders, B., et al., 2016. A high resolution coupled hydrologic-hydraulic model (HiResFlood-UCI) for flash flood modeling. J. Hydrol. 541, 401–420. https://doi.org/10.1016/j.jhydrol.2015.10.047.

Ni, Y., Cao, Z., Liu, Q., Liu, Q., 2020. A 2D hydrodynamic model for shallow water flows with significant infiltration losses. Hydrol. Process. 34 https://doi.org/10.1002/hyp.13722.

Pontes, P.R.M., Fan, F.M., Fleischmann, A.S., de Paiva, R.C.D., Buarque, D.C., Siqueira, V.A., et al., 2017. MGB-IPH model for hydrological and hydraulic simulation of large floodplain rivers systems coupled with open source GIS. Environ. Model. Software 94, 1–20. https://doi.org/10.1016/j.envsoft.2017.03.029.

Sampson, C.C., Smith, A.M., Bates, P., Neal, J.C., Alfieri, L., Freer, J.E., 2015. A high-resolution global flood hazard model. Water Resour. Res. 51, 7358–7381. https://doi.org/10.1002/2015WR016954.

Sanders, B., 2007. Evaluation of on-line DEMs for flood inundation modelling. Adv. Water Resour. 30, 1831–1843. https://doi.org/10.1016/j.advwatres.2007.02.005.

Schumann, G.J.P., Bates, P.D., 2018. The need for a high-accuracy, open-access global DEM. Front. Earth Sci. 6, 225. https://doi.org/10.3389/feart.2018.00225.

Sebastian, A., Bader, D.J., Nederhiff, C.M., Leijnse, T.W.B., Bicker, J.D., Aarninkhof, S.G., 2021. Hindcast of pluvial, fluvial, and coastal flood damage in Houston, Texas during Hurricane Harvey (2017) using SFINCS. Nat. Hazards. https://doi.org/10.1007/s11069-021-04922-3.

Smith, R.E., Hebbert, R.H.B., 1979. A Monte Carlo Analysis of the hydrologic effects of spatial variability of infiltration. Water Resour. Res. 15 (2), 419–429. https://doi.org/10.1029/WR015i002p00419.

Swain, D.L., Wing, O.E.J., Bates, P.D., Done, J.M., Johnson, K.A., Cameron, D.R., 2020. Increased flood exposure due to climate change and population growth in the United States. Earth's Future 8. https://doi.org/10.1029/2020EF001778 e2020EF001778.

Tabari, H., 2020. Climate change impact on flood and extreme precipitation increases with water availability. Sci. Rep. 10, 13768 https://doi.org/10.1038/s41598-020-70816-2.

Tang, G., Clark, M.P., Papalexiou, S.M., Ma, Z., Hong, Y., 2020. Have satellite precipitation products improved over last two decades? A comprehensive comparison of GPM IMERG with nine satellite and reanalysis datasets. Rem. Sens. Environ. 240, 111697 https://doi.org/10.1016/j.rse.2020.111697.

Teng, J., Jakeman, A.J., Vaze, J., Croke, B.F.W., Dutta, D., Kim, S., 2017. Flood inundation modelling: a review of methods, recent advances and uncertainty analysis. Environ. Model. Software 90, 201–216. https://doi.org/10.1016/j.envsoft.2017.01.006.

Triet, N.V.K., Dung, N.V., Hoang, L.P., Duy, N.L., Tran, D.D., Anh, T.T., Apel, H., 2020. Future projections of flood dynamics in the Vietnamese Mekong Delta. Sci. Total Environ. 742, 140596 https://doi.org/10.1016/j.scitotenv.2020.140596.

Viero, D.P., Rober, G., Matticchio, B., Define, A., Tarolli, P., 2019. Floods, landscape modifications and population dynamics in anthropogenic coastal lowlands: the Polesine (northern Italy) case study. Sci. Total Environ. 651, 1435–1450. https://doi.org/10.1016/j.scitotenv.2018.09.121.

Viterbo, F., Mahoney, K., Read, L., Salas, F., Bates, B., Elliott, J., Cifelli, R., 2020. A multiscale, hydrometeorological forecast evaluation of National water model forecasts of the may 2018 ellicott city, Maryland, flood. J. Hydrometeorol. 21 (3), 475–499. https://doi.org/10.1175/JHM-D-19-0125.1.

Wing, O.E.J., Bates, P.D., Sampson, C.C., Smith, A.M., Johnson, K.A., Erickson, T.A., 2017. Validation of a 30 m resolution flood hazard model of the conterminous United States. Water Resour. Res. 53, 7968–7986. https://doi.org/10.1002/2017WR020917.

Woolhiser, D.A., Smith, R.E., Giraldez, J.V., 1996. Effects of spatial variability of saturated hydraulic conductivity on hortonian overland flood. Water Resour. Res. 32, 671–678. https://doi.org/10.1029/95WR03108.

Xue, X., Hong, Y., Limaye, A.S., Gourley, J.J., Huffman, G.J., Khan, S.I., Doriji, C., Chen, S., 2013. Statistical and hydrological evaluation of TRMM-based Multi-satellite Precipitation Analysis over the Wangchu Basin of Bhutan: are the latest satellite precipitation products 3B42V7 ready for use in ungauged basins? J. Hydrol. 499, 91–99. https://doi.org/10.1016/j.hydrol.2013.06.042.

Yamazaki, D., Kanae, S., Kim, H., Oki, T., 2011. A physically based description of floodplain inundation dynamics in a global river routing model. Water Resour. Res. 47, W04501 https://doi.org/10.1029/2010WR009726.

Yang, G., Bowling, L.C., Cherkauer, K.A., Pijanowski, B.C., 2011. The impact of urban development on hydrologic regime from catchment to basin scales. Landsc. Urban Plann. 103 (2), 237–249. https://doi.org/10.1016/j.landurbplan.2011.08.003.

Yussouf, N., Wilson, K.A., Martinaitis, S.M., Vergara, H., Heinselman, P.L., Gourley, J.J., 2020. The coupling of NSSL warn-on-forecast and FLASH systems for probabilistic flash flood prediction. J. Hydrometeorol. 21 (1), 123–141. https://doi.org/10.1175/JHM-D-19-0131.1.

Zhao, R.J., 1995. The Xinanjiang Model. *Computer Models of Watershed Hydrology*, pp. 215–232.

Zhang, J., Lin, P., Gao, S., Fang, Z., 2020. Understanding the re-infiltration process to simulating streamflow in North Central Texas using the WRF-hydro modeling system. J. Hydrol. 587, 124902 https://doi.org/10.1016/j.jhydrol.2020.124902.